PFC/JA-86-32

ELECTRON MICROINSTABILITIES IN AN RF-HEATED, MIRROR-CONFINED PLASMA

Garner, R.C.; Mauel*, M.E.; Hokin, S.A.;
Post, R.S.; Smatlak, D.L.

May 1986

Plasma Fusion Center
Massachusetts Institute of Technology
Cambridge, Massachusetts 02139 USA

*present address: Columbia University, New York, N.Y.

Submitted for publication in: Physical Review Letters.

ABSTRACT

Two types of electron microinstability are observed in the ECRH plasma of the Constance B mirror experiment. The first has been identified as the whistler instability and the second is either a fast electromagnetic wave instability or the upper hybrid loss cone instability. We present experimental evidence which indicates that both instabilities are driven by a warm population of electrons (.15-3 keV) while the hot component (T=400 keV) is stable and has little effect on microinstability. We show that calculations which identify the whistler instability support this conclusion if a relativistic formulation is considered.

A plasma characterized by a non-Maxwellian electron velocity space distribution function may be subject to electron microinstability. In a hot electron, mirror confined plasma the whistler instability and the upper hybrid loss cone instability are driven by temperature anisotropy.[1,2] The cyclotron maser instability is driven by population inversion.[3] Mirror experiments in which the electrons are heated by electron cyclotron resonance heating (ECRH) have demonstrated the existence of microinstabilites.[4, 5,6,7] In these experiments rf emission in the electron cyclotron range of frequencies is observed and is typically accompanied by enhanced particle endloss induced by the unstable waves. While the frequency spectrum and power of the rf emission has been measured in many cases, less emphasis has been placed on determining which regions of velocity space drive microinstability. Theoretical investigations based on the Vlasov dispersion relation have been used to identify the experimentally observed instabilities.[1,2,3,8,9,10] The equilibrium distribution functions used in most of these cases do not describe the velocity space diffusion that electrons undergo in response to ECRH.

We show that the two electron microinstabilities which are exhibited by the plasma of the Constance B mirror experiment, the whistler instability and an unidentified one which we refer to as the type 2 instability,[11] are mainly driven by warm electrons, while the hot electrons are stable and do not contribute to wave growth. Our theoretical model, which uses a distri-

bution function that describes ECRH diffusion, supports this conclusion. It identifies the experimentally observed whistler instability and, unlike the situation for a bi-Maxwellian distribution,[10] predicts that a sufficiently hot plasma is stable if a relativistic formulation is considered.

Constance B is a quadrupole magnetic mirror experiment in which a hydrogen plasma is produced and heated by 1 kW of rf at 10.5 GHz. The nonrelativistic cyclotron frequency on axis at the midplane is 8.4 GHz. Two distinct electron energy components are detected. Electrostatic gridded endloss analyzers detect a constant 150 eV cold electron component which is confined electrostatically by the 150 volt plasma potential. Ge and NaI x ray detectors, which measure bremsstrahlung photons with energies greater than 2 keV, identify a hot electron component which is heated at 450 keV/sec until a 400 keV steady state temperature is attained. Although not directly identified, the endloss analyzers suggest that a warm 1.5−2 keV component exists. The electrons in this energy regime drive the electron microinstabilities, as we show below. An interferometer indicates that the hot component contributes approximately two thirds of the total line density of 3.5×10^{12} cm^{-2}. The midplane plasma diameter is 20 cm.

The two instabilities are each associated with a different type of rf emission, both emitted at power levels greater than the 1 Watt cyclotron emission. The rf emission associated with the whistler instability occurs in fairly regular, intense bursts (period $\sim$ 600 μsec, energy per burst $\sim$ 5×10^{-6}

Joules, burst time $\sim$ 5 μsec) with frequencies in the range 6.7$-$8.7 GHz. It correlates with bursts of electron and ion endloss, diamagnetism, and potential fluctuations.[12] The rf associated with the type 2 instability is seen continuously (average power $\sim$ 10 Watts) and is associated with a continuous enhanced endloss. It has frequencies in the range between 8.7 GHz and the heating frequency, 10.5 GHz. Both instabilities appear simultaneously for gauge pressures above 5×10^{-7} torr. Below this pressure only the whistler instability occurs.

The following evidence shows that both microinstabilities are driven by the warm electrons while the hot component is stable and has little effect on microinstability:

1) The average unstable rf emission power, shown in Fig. 1(b) as a function of pressure 1.3 sec after ECRH begins, is constant in time during ECRH whereas the hot electron parameters vary in time, as shown in Fig. 2. Fig. 1 also shows that the plasma diamagnetism and the unstable rf emission power peak at different values of gas pressure.

2) The whistler emission begins less than 1 msec after the gas breaks down and the type 2 emission begins less than 5 msec after the gas breaks down. The temperature determined from the x ray spectrum is only 10 keV 20 msec after the gas breaks down.

3) The type 2 emission completely stops approximately 5 msec after ECRH is turned off. The whistler emission bursts sporadically for several

milliseconds after ECRH is turned off and then completely stops. The endloss analyzers indicate that the electrons with energies less than 5 keV, which are responsible for more than 99% of the total electron endloss current, leave within approximately 5 msec after ECRH is turned off, the same amount of time it would take a 1.2 keV Maxwellian of the same density to collisionally decay. The x ray detector indicates that the hot electron temperature does not change after ECRH is turned off and the diamagnetic loop together with the x ray detector indicates that hot electron density decays exponentially with a 1 sec time constant.

4) There is no unstable rf emission from a plasma which contains just a hot electron component. Such a plasma can be produced by turning off the neutral gas during the shot while leaving the ECRH on (see Fig. 3).

The conclusion that the warm electrons drive the microinstabilities leads to conclusions about the experimentally measured microinstability induced electron endloss. The endloss analyzers indicate that 99% of the microinstability induced electron endloss consists of particles with energies less than 5 keV and with average energy of 1.5 keV (these particles are responsible for approximately half of the total time-averaged particle loss rate). The unstable wave energy comes primarily from these particles. A scintillator probe indicates that $30 - 50\%$ of the hot electron endloss is caused by interactions with the unstable waves while the remainder is caused almost entirely by interactions with the ECRH waves. Since the hot electrons do

not drive microinstability this implies that hot electrons gain energy from the unstable waves as well. However, there is a net energy loss because the hot electrons which diffuse downward in energy have a chance to enter the loss cone and carry their total energy out of the plasma.

Dispersion relation calculations identify the whistler instability and indicate that a sufficiently hot component is stable if a relativistic formulation is used. We have done calculations, which predict electromagnetic wave instabilities, in a manner similar to Lee and Wu,[8] except our treatment is fully relativistic and we have used the following equilibrium electron velocity space distribution function:

$$f_0(E,\mu) = exp\left[-\frac{\chi}{T_\chi} - \theta(\eta)\frac{\eta}{T_{\eta+}} + \theta(-\eta)\frac{\eta}{T_{\eta-}}\right] \qquad (1)$$

where $\chi = \frac{1}{2}(E+\mu B_h)$, $\eta = \frac{1}{2}(E-\mu B_h)$, E is the particle kinetic energy, μ is the magnetic moment, $\theta(\eta)$ is the unit step function, $B_h = \omega_h m_o c/e$, and ω_h is the applied ECRH frequency. The lines defined by $\eta = constant$ are the diffusion paths for waves with frequency ω_h. Contours of this function are plotted in Fig. 4(a). They closely resemble the contours of distribution functions which are numerically generated by Fokker-Planck simulations of ECRH, mirror confined plasmas.[13] Unlike distributions used in the past, Eq. (1) reflects the velocity space diffusion that such electrons undergo in response to the heating waves. It does not allow for unstable waves with frequency above the ECRH frequency, which agrees with experiment. The region defined by $\eta > 0$ is destabilizing for a wave and the region defined

by $\eta < 0$ is stabilizing for a wave.

Local dispersion relation calculations were done for a range of locations along the axial magnetic field line and for a range of wave frequencies. Fig. 4(b) shows the contours of $f_i = \omega_i/2\pi$ for a particular choice of the parameters. The vertical axis gives the local nonrelativistic cyclotron frequency, with 8.4 GHz the midplane cyclotron frequency. The horizontal axis gives the wave frequency. For this calculation $k_\perp$ is set to zero so that the whistler waves are considered. The unstable wave frequencies predicted by this calculation are in good agreement with the frequencies of the unstable whistler waves observed in the experiment.

Fig. 5 shows a plot of the growth rate f_i as a function of the temperature parameters, T_χ, $T_{\eta+}$, and $T_{\eta-}$, where the ratios between each were kept constant. Both relativistic and nonrelativistic calculations were done and are included in Fig. 5 for comparison. The stability of a sufficiently hot component predicted by the relativistic formulation is due to the bending of the characteristic line ($\eta = 0$) separating the stabilizing region from the destabilizing region so that there are more resonant particles which take energy from the wave than give energy to it. This is to be contrasted to the work of Tsang,[10] who uses a bi-Maxwellian distribution and shows that ω_i continues to increase as temperature increases, although the increase is less in the relativistic formulation than in the nonrelativistic formulation.

In summary, we have described the two electron microinstabilities that are exhibited by the ECRH, mirror confined plasma of the Constance B experiment and have concluded from the experimental data that the warm electrons drive the microinstabilities while the hot component is stable and has little effect. We have shown that a relativistic Vlasov dispersion relation calculation supports this conclusion for the whistler instability.

This work was supported by the U. S. Department of Energy, Contract No. DE-AC02-78ET51013.

References

[a] Current address: Dept. of Applied Physics, Columbia University, New York, N.Y. 10027.

[1]N. T. Gladd, Phys. Fluids **26**, 974 (1983).

[2]M. Porkolab, Phys. Fluids **27**, 162 (1984).

[3]Y. Y. Lau and K. R. Chu, Phys. Rev. Lett. **50**, 243, (1983).

[4]R. A. Blanken and N. H. Lazar, Phys. Fluids **13**, 2752 (1970).

[5]H. Ikegami, H. Ikezi, M. Hosokawa, K. Takayama, and S. Tanaka, Phys. Fluids **11**, 1061 (1968).

[6]R. A. James, R. F. Ellis, and C. J. Lasnier, Bulletin of the American Physical Society **29**, 1187 (1984).

[7]J. H. Booske, W. D. Getty, and R. M. Gilgenbach, Phys. Fluids **28**, 3116 (1985).

[8]L. C. Lee and C. S. Wu, Phys. Fluids **23**, 1348 (1980).

[9]H. K. Wong, C. S. Wu, F. J. Ke, R. S. Schneider, and L. F. Ziebell, J. Plasma Physics **28**, 503 (1982).

[10]K. T. Tsang, Phys. Fluids **27**, 1659 (1984).

[11]The type 2 instability is either a fast electromagnetic wave instability, as suggested by our theory, or the upper hybrid loss cone instability, as suggested by work done by Porkolab.[2]

[12]These same bursts have been seen in Refs. 4 and 6.

[13]M. E. Mauel, Phys. Fluids **27**, 2899 (1984).

Figures

FIG. 1. (a) The diamagnetic flux and (b) the power of the total unstable rf emission as a function of the gauge pressure during ECRH. The gauge pressure is useful because it is a known parameter through which measured parameters can be compared. Each point is associated with a different shot and corresponds to the average over a 40 msec time span 1.3 sec after ECRH begins. The total unstable rf emission power is approximately constant during the entire heating phase of the shot, whereas the diamagnetic flux increases (see Fig. 2).

FIG. 2. Data from a shot with 1 kW ECRH power and 5×10^{-7} Torr gauge pressure. (a) The temperature of hot electrons is determined by unfolding the x ray spectrum with a Maxwellian distribution, every 100 msec. (b) Diamagnetic flux. (c) Power of total unstable rf emission. (d) Line density.

FIG. 3. Data showing the stability of the hot component. The gas is turned off at .6 sec while the ECRH is left on until 2 sec. The hot component has the longest confinement and remains for several seconds after the cold and warm components have decayed. There is no unstable rf emission during this time. (a) Hot electron temperature. (b) Diamagnetic flux. (c) Power of total unstable rf emission. (d) Gauge pressure.

FIG. 4. (a) Contours of Eq. 1 in relativistic velocity space for $T_\chi = 10$ keV,

$T_{\eta+} = 5$ keV, and $T_{\eta-} = .25$ keV. (b) Contours of f_i using these temperature parameters. The vertical axis is the local cyclotron frequency and corresponds to the position along a field line. The horizontal axis is the real frequency of a wave that satisfies the cold plasma dispersion relation with $k_\perp = 0$.

FIG. 5. (a) The real and (b) the imaginary parts of the frequencies corresponding to the most unstable whistler waves for different values of T_χ, with $T_\chi/T_{\eta+} = 2$ and $T_\chi/T_{\eta-} = 20$ held constant. (These are the maximum contours of plots like the one in Fig. 4b.) For these parameters the average particle kinetic energy is $1.05T_\chi$.

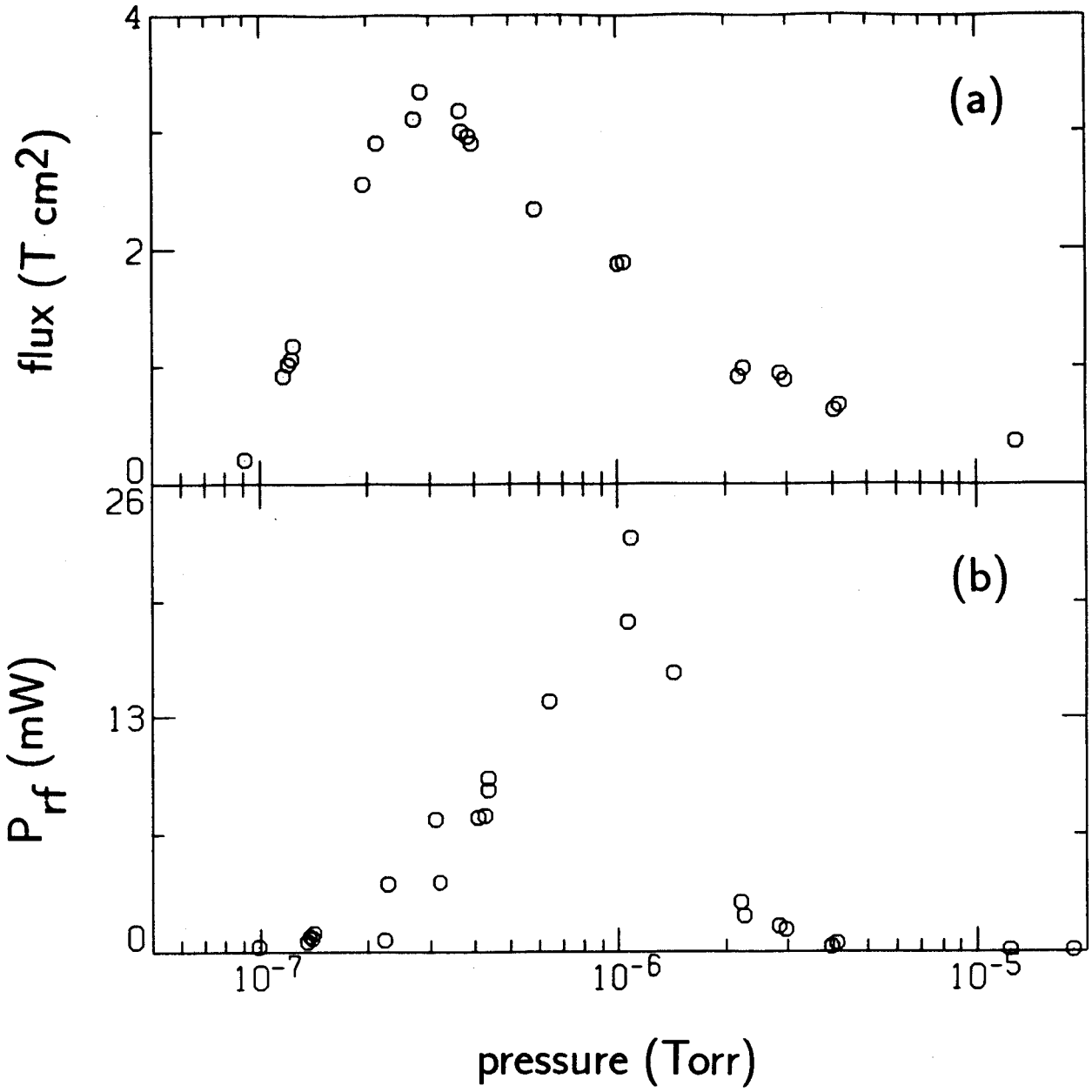

Fig. 1

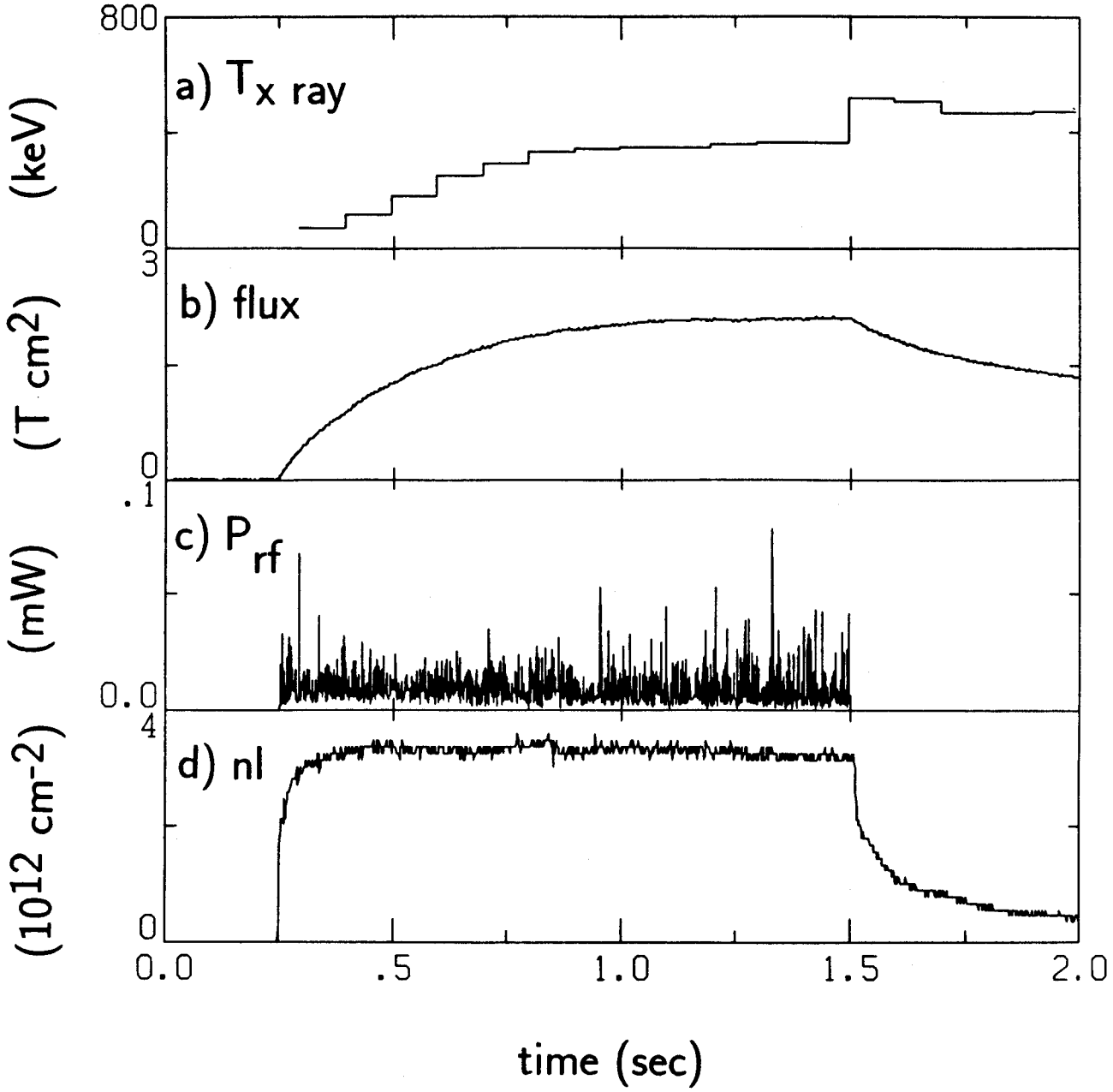
800
a) $T_{x\ ray}$
(keV)
0
3
b) flux
(T cm2)
0
.1
c) P_{rf}
(mW)
0.0
4
d) nl
(1012 cm-2)
0
0.0
.5
1.0
1.5
2.0
time (sec)

Fig. 2

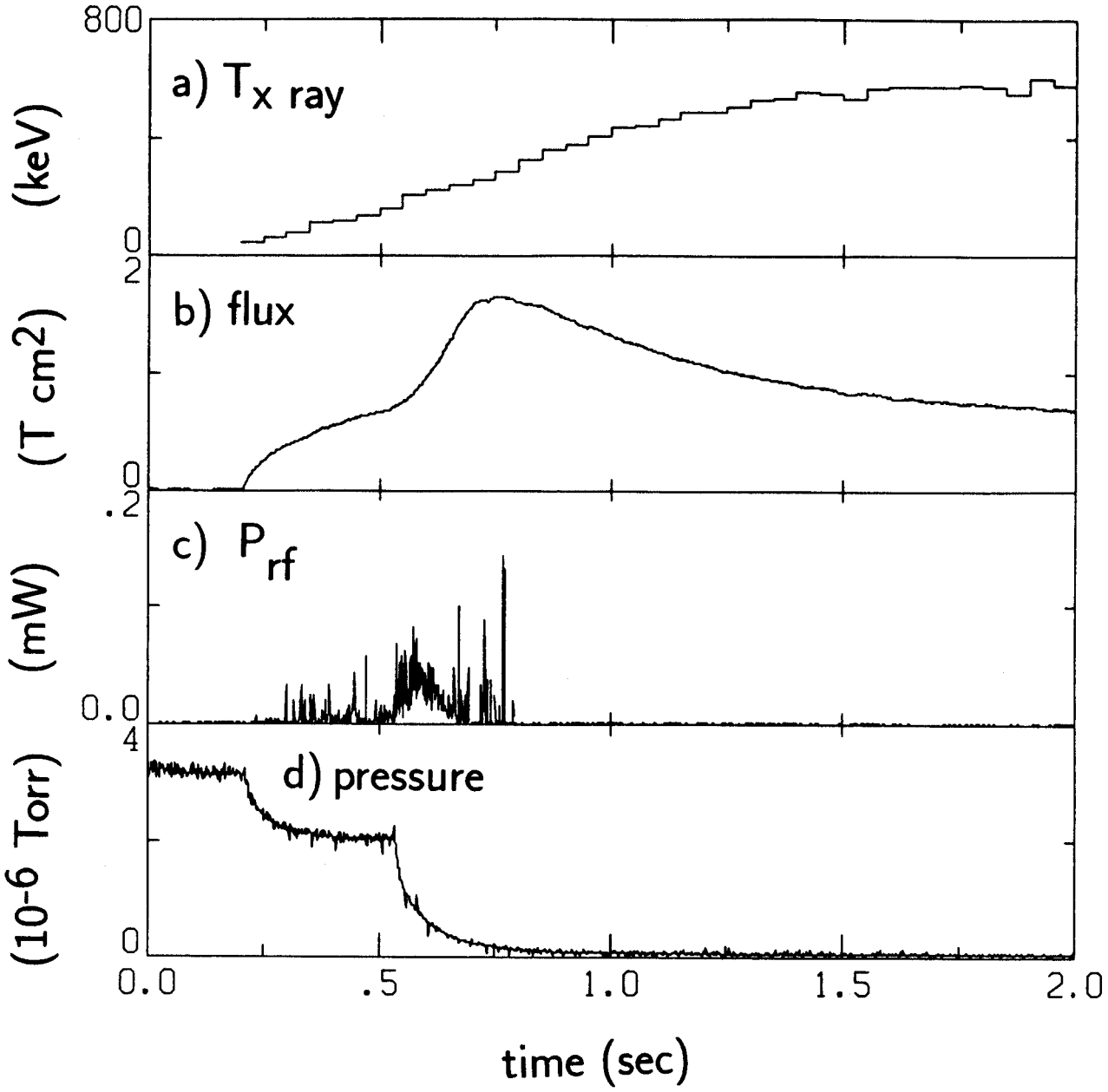
800
a) $T_{x\ ray}$
(keV)
0
2
b) flux
(T cm2)
0
.2
c) P_{rf}
(mW)
0.0
4
d) pressure
(10-6 Torr)
0
0.0
.5
1.0
1.5
2.0
time (sec)

Fig. 3

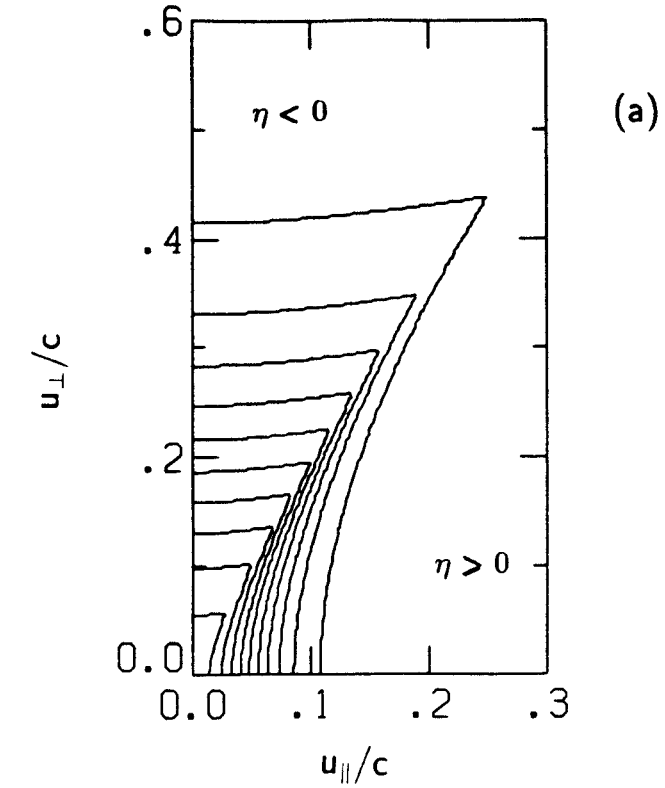
.6
.4
.2
0.0
0.0
.1
.2
.3
$u_\perp/c$
$u_\parallel/c$
$\eta < 0$
$\eta > 0$
(a)

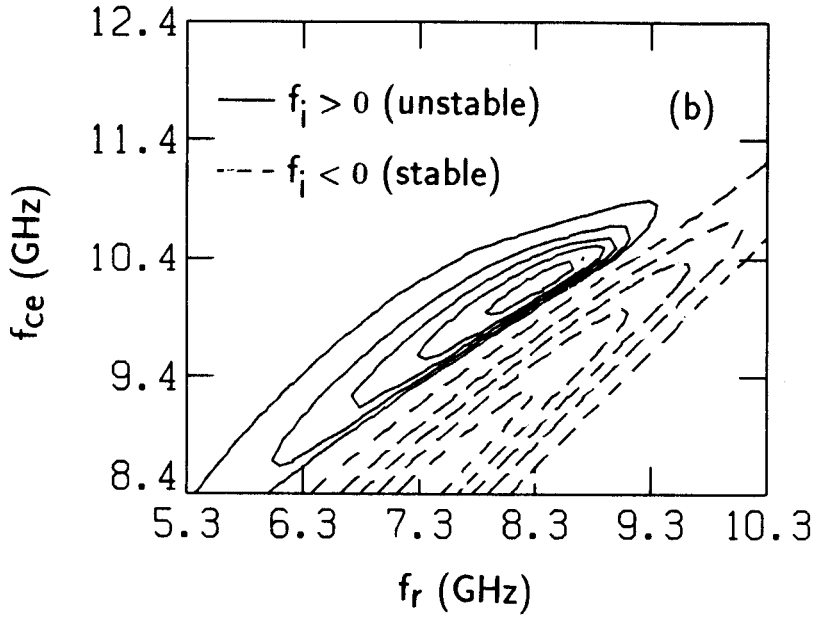
12.4
11.4
10.4
9.4
8.4
5.3
6.3
7.3
8.3
9.3
10.3
f_{ce} (GHz)
f_r (GHz)
$f_i > 0$ (unstable)
$f_i < 0$ (stable)
(b)

Fig. 4

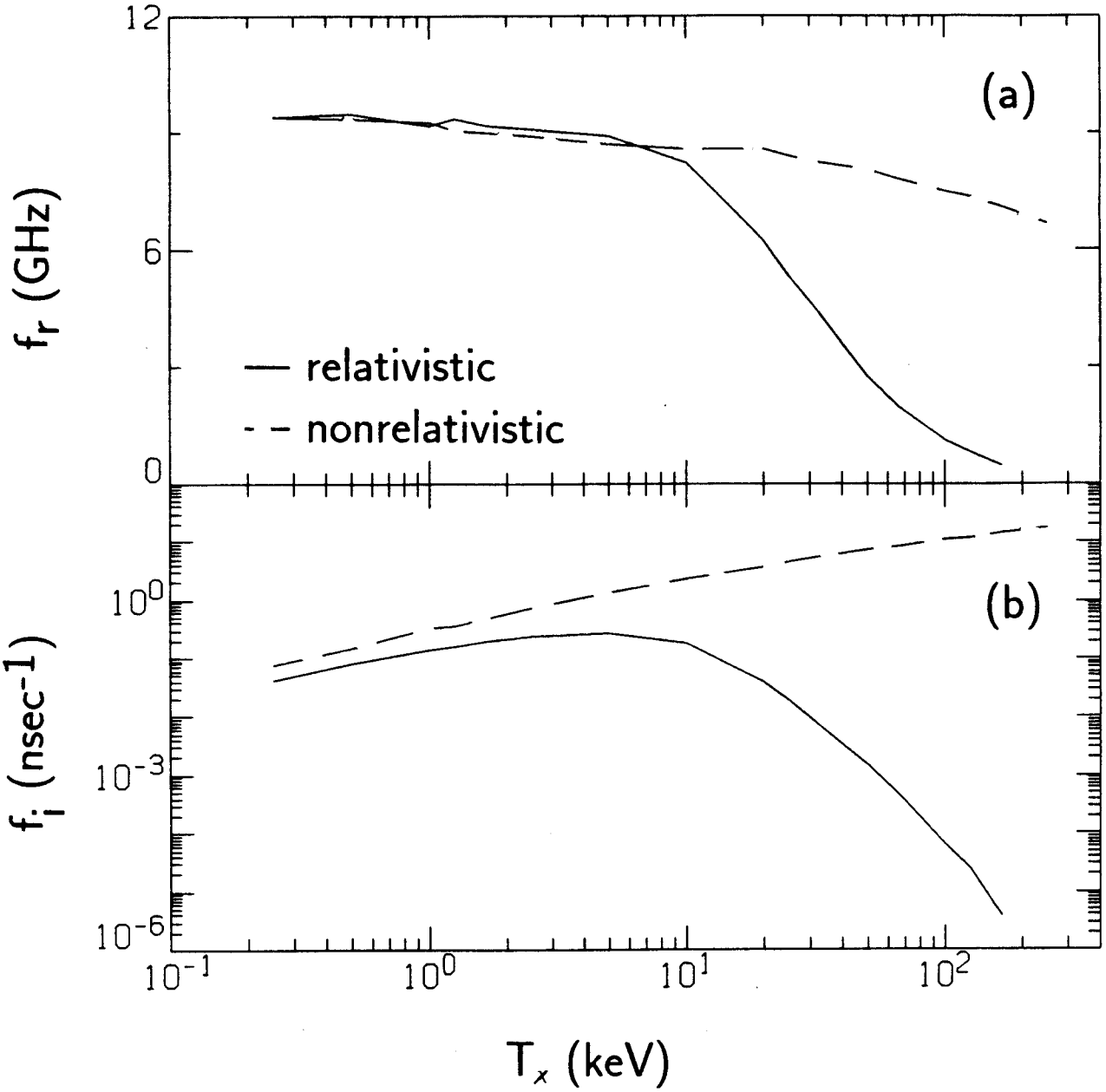
12
6
0
(a)
— relativistic
- - nonrelativistic
f_r (GHz)
10^0
10^{-3}
10^{-6}
(b)
f_i (nsec^{-1})
10^{-1}
10^0
10^1
10^2
T_x (keV)

Fig. 5